INTERNATIONAL ATOMIC ENERGY AGENCY
UNITED NATIONS EDUCATIONAL, SCIENTIFIC AND CULTURAL ORGANIZATION
INTERNATIONAL CENTRE FOR THEORETICAL PHYSICS
I.C.T.P., P.O. BOX 586, 34100 TRIESTE, ITALY. CABLE CENTRATOM TRIESTE

UNITED NATIONS INDUSTRIAL DEVELOPMENT ORGANIZATION
INTERNATIONAL CENTRE FOR SCIENCE AND HIGH TECHNOLOGY

SMR.550 - 11

SPRING COLLEGE IN MATERIALS SCIENCE ON
"NUCLEATION, GROWTH AND SEGREGATION IN MATERIALS
SCIENCE AND ENGINEERING"
(6 May - 7 June 1991)

STABILITY OF MICROSCOPIC CLUSTERS
(PART II)

J.A. ALONSO
Departamento de Fisica Teorica y Fisica Atomica y Nuclear
Facultad de Ciencias
Universidad de Valladolid
Valladolid
Spain

STABILITY OF MICROSCOPIC CLUSTERS

2nd Lecture: Shell effects in clusters of simple metallic elements

J. A. ALONSO

Lectures to be delivered at:
Spring College in Materials Science on
"Nucleation, growth and segregation in Materials Science and Engineering"
(International Centre for Theoretical Physics, Triestre, May-June 1991)

1. INTRODUCTION. EXPERIMENTS ON CLUSTERS OF SMALL OR INTERMEDIATE SIZE[1]

Sodium vapour , or other alkaline elements, can be expanded supersonically from a hot stainless steel oven with a fine exit nozzle, resulting in well focussed cluster beams. The oven can be pressurized with excess argon to improve the performance. In the tiny expansion zone, terminating some tenths of a millimeter beyond the nozzle, clusters form as a result of collisions between Na atoms. The clusters will warm up because of the heat of condensation, and so there will be a tendency for evaporation from the clusters also. As the expansion proceeds, collisions between Na atoms cease to take place and now the tendency for evaporation will dominate. Each cluster will loose mass and cool as time goes on. In the evaporation chains, clusters with low evaporation rates, i.e. strong binding energy of the least bound atom, will tend to pile up. After entering a vacuum zone and a flight of about one millisecond duration, the clusters can be gently ionized with ultraviolet light, and mass analyzed.

In 1984, W.D. Knight and his coworkers in Berkeley performed an experiment of that kind[2]. They found an abundance distribution as shown in Figure 1. There are prominent abundance maxima and/or steps at N = 8, 20, 40, 58 and 92. The arguments given above indicate that clusters composed of 8, 20, 40, 58 and 92 atoms are especially stable. Since Na is a monovalent atom the number of electrons in these clusters is 8, 20, 40, 58 and 92 respectively. Similar experiments have confirmed the same magic numbers in the mass spectra of other alkaline elements (Li^1, K^3, Rb^4 and Cs^5). Furthermore, measurements of the ionization potential[1], IP, of Potassium clusters as a function of size N show that the value of IP drops abruptly from N to N+1 at precisely the values N = 8, (18), 20, 40, 58 and 92, that is,

the magic numbers, with the addition of N = 8 (see Fig. 2). The ionization potential, which is the energy necessary to extract the least bound electron from the cluster, will be discussed in detail elsewhere. Fig. 2 thus shows that the electrons are more tightly bound in magic clusters.

One can also infer cluster stabilities from dissociation energies in fragmentation experiments[6]. In a typical photodissociation experiment, cluster ions like Na_N^+ are excited by laser light to a highly excited state $(Na_N^+)^*$

$$Na_N^+ + h\upsilon \rightarrow (Na_N^+)^* . \qquad (1)$$

The excited cluster can evaporate a neutral atom (or in general a fragment Na_p)

$$\left(Na_N^+\right)^* \rightarrow Na_{N-p}^+ + Na_p \qquad (2)$$

if enough excitation energy is localized in a single vibrational mode so as to overcome the binding energy D_p of the fragment:

$$D_p = E\left(Na_{N-p}^+\right) + E\left(Na_p\right) - E\left(Na_N^+\right) > 0. \qquad (3)$$

Starting from the excited cluster $(Na_N^+)^*$ in which the internal excitation energy E^* is randomly distributed among the s = 3N-6 internal vibrational modes, the classical expression for the probability of localizing enough energy into a single mode so as to overcome the fragment binding energy D_p is $\left[(E^* - D_p) / E^* \right]^{s-1}$, and the rate of dissociation is given by

$$k = \tau^{-1} = \nu g \left[(E^* - D_p) / E^* \right]^{s-1} . \qquad (4)$$

In this equation g is the number of surface atoms and ν is their vibrational frequency. τ^{-1} is the reciprocal of the dissociation time. This equation can be used together with experimental information on

the fraction of dissociated clusters to obtain the binding energy D_p. Figure 3 shows the results obtained by Bréchignac et al[6] for the dissociation energies of Na_N^+ and K_N^+. An important point about this Figure is that the dissociation energies plotted are those for the lowest dissociation channel. This channel corresponds to the evaporation of the fragment (Na_p or K_p) with the smallest binding energy, which as eq. (4) shows is the most probable dissociation channel. For the clusters studied, Na_N^+ and K_N^+, this is the monomer (Na,K) in most cases, and only in a few cases with small N the least bound fragment is the dimer (Na_2, K_2). However, the most relevant conclusion obtained from figure 3 is the occurrence of abrupt drops of the dissociation energy between Na_9^+ and Na_{10}^+ and between Na_{21}^+ and Na_{22}^+ and similarly for the K case. Notice that the photodissociation experiment is performed on ionized clusters, in which the number of electrons is N_e = N-1. Thus, high binding energies occur for clusters with 8 and 20 electrons. The dissociation experiments, first of all corroborate the magic numbers obtained in the abundance spectra and, second, unambiguously indicate that the magic character is associated with the number of valence electrons in the cluster, and not with the number of ions. The same conclusion is evidently deduced from the ionization potentials or from the mass spectra of clusters directly produced in an ionized state[5]. Dissociation experiments have also been performed in which the excitation is produced by collisions with rare-gas ions. These lead to the same conclusions as photodissociation experiments.

2. SHELL MODEL

The magic numbers observed in alkali clusters are completely different from those observed in inert gas clusters. On the other hand we have seen at the end of Section 1 that the former ones are due to electronic effects. Knight and coworkers[2] noticed that their experimental results can be explained by a shell-model. Figure 4 shows the energy level spectra obtained by solving Schrödinger's equation for electrons confined in some simple three-dimensional spherically symmetric potential wells: (a) a three-dimensional isotropic harmonic oscillator, (b) a three-dimensional square-well (inside the well the potential has a particular constant value, and outside it another constant value), (c) an intermediate potential between them. The figure shows that confinement of the electrons to an spherical region leads to shell structure. For a three-dimensional harmonic oscillator model the energy levels are equally spaced; degenerate levels are separated by wide gaps. A similar result is found for a three-dimensional square-well potential, but with unevenly spaced energy levels.

In general energy levels for electrons bound in a spherically symmetric potential are characterised by radial and angular momentum quantum numbers, k and l respectively. k - 1 is equal to the number of nodes in the radial wave function. The successive energy levels (and their degeneracies) for the square well potential are 1s(2), 1p(6), 1d(10), 2s(2), 1f(14), 2p(6), 1g(18), 2d(10), 1h(22), 3s(2), 2f(14), 1i(26), 3p(6), 2g(18),... Fixed k and l, the magnetic quantum number can take the values m = l, l-1, ... -l, and the spin quantum number two values s = + 1/2 and - 1/2. This gives the total degeneracy 2(2l+1) for an (k,l) level. Hence, as electrons fill the shells, closings occur for total electron numbers, 2, 8, 18, 20, 34, 40,

58, 68, 90, 92, 106, 132, 138, 156 and so on. In clusters of alkali metals each atom contributes one valence electron, and shell closures occur for clusters containing the number of electrons in this series. We know from atomic physics that closed-shell configurations are stable, because of the energy gaps between electronic shells. The same effect certainly operates in the case of the simple models of Figure 4. In the list of shell-closing numbers of the square well potential we already recognize the magic numbers of the alkaline clusters, plus other shell-closing numbers not observed in the experiments. Two reasons contribute to the discrepancy. First, only a large gap to the next shell enhances the stability of a closed shell. Second, the simple square well is only an approximate model. A potential intermediate between the harmonic oscillator and the square well, like the Woods-Saxon potential[7] produces a level spectra with improved features, for instance a much smaller gap between the 1f and 2p shells.

Although the shell model is familiar from the atom and nucleus, it is remarkable how well it works for clusters of the alkaline metals. This is however, not too surprising. Solid state physicists are familiar with the free and nearly-free electron models of simple metals[8]. The essence of these models is to realize that the effective potential seen by the conduction electrons in metals like Na, K, etc. is nearly constant through the volume of the metal. This is so because (a) the ion cores occupy only a small fraction of the atomic volume, and (b) the effective ionic potential is weak. Under these circumstances a constant potential in the interior of the metal is a good approximation. Electrons cannot spontaneusly escape from the metal. In fact the energy needed to extract one electron through the surface is called the work function, W_f. This means that the potential rises abruptly at the surface of the metal. Now if the metal piece is microscopic, one sees that the potential seen by the electrons in a small alkali particle is like that given in the middle of Figure 4.

3. SPHERICAL JELLIUM MODEL[1]

The model potentials discussed in Section 2 already give a qualitative explanation of the magic numbers observed in alkali metal clusters. For more quantitative purposes one needs a better, self-consistent, potential. The spherical jellium model provides a simple way to generate such a self-consistent potential. In this model the background of positive ions is smeared out over the volume of the cluster, that is, we consider a positive charge density distribution

$$n_+(\vec{r}) = \begin{cases} n_0 & , \ r < R \\ 0 & , \ r > R . \end{cases} \tag{5}$$

Here R is the radius of the cluster, related to the number of atoms N by the equation

$$\frac{4}{3}\pi R^3 = N\Omega, \tag{6}$$

where Ω is the volume per atom in the macroscopic metal. The constant positive density n_0 is related to Ω and to the valence Z (Z = 1 for alkaline elements) by

$$Z = n_0 \Omega. \tag{7}$$

This positive background provides the external potential V_{ext}. Density functional theory[9] is then used to calculate the electronic distribution of interacting electrons in this external potential. This is achieved by solving the single-particle equations

$$\left(-\frac{1}{2}\nabla^2 + V_{eff}(\vec{r}) \right) \phi_i(\vec{r}) = \varepsilon_i \phi_i(\vec{r}) \tag{8}$$

which lead to the electron density

$$n(r) = \sum_{i=1}^{N} | \phi_i(\vec{r}) |^2 . \qquad (9)$$

The effective potential in equation (8) represents the average effect of the attraction from the ions and the repulsion from the other electrons. It is given by

$$V = V_{ext} + V_H + V_{xc} . \qquad (10)$$

V_H is the classical electrostatic potential of the electronic cloud

$$V_H(r) = \int \frac{n(r')}{|\vec{r} - \vec{r}'|} d^3r' , \qquad (11)$$

and V_{xc} is the exchange and correlation part. Exchange takes care of Pauli exclusion principle which forbids that two electrons simultaneously occupy the same quantum state. The correlation piece takes into account electronic correlations beyond the Pauli principle: the electrical repulsion between electrons has the effect that one electron forbids the presence of other electrons in its close neighbourhood. Exchange an correlation effects can be visualized as a hole around an electron (indicating that other electrons are missing from its close neighbourhood) which accompanies the electron as it moves through the system (see Fig. 5)

Normally $V_{xc}(\vec{r})$ is calculated using the Local Density approximation (LDA). This means that V_{xc} at point $\vec{r}$ is assumed to depend only on the local electron density at $\vec{r}$, that is, $n(\vec{r})$ (see technical details in ref. 9).

The jellium model has been applied to alkaline metal clusters by many authors (see ref.1). Figure 6 shows the self-consistent electron potential calculated for a spherical sodium cluster with twenty atoms. The degenerate levels are filled up to electron number N= 20. In a spherical cluster with 21 electrons the last electron will have to fill one of the 1f levels above (dashed line). This electron is less bound, by at least 0.5 eV, compared to the 20 th electron, and should be easier to remove by photo-ionization. This explains why the ionization potential drops with the opening of a new shell (see Fig. 2). The total energy of the cluster E(N) can also be calculated (see technical details in ref.9). The total energy per atom, E(N)/N, is plotted in Fig. 7 for Sodium as a function of cluster size. It is a smooth curve except for kinks at N = 8, 18, 20, 34, 40, 58, 92, ... where the total energy changes abruptly. The bulk limit is expected to be around -2.2 eV. To examine the abrupt changes in the total energy we define a quantity

$$\Delta_2(N) = E(N+1) + E(N-1) - 2E(N), \qquad (12)$$

which is related to the second derivative of the energy with respect to N, and represents the relative binding energy for a cluster with N atoms compared to clusters with (N+1) and (N-1) atoms. If an energy level is just filled by the electrons in a cluster of N atoms and the next available level is separated from this filled level by a perceivable energy gap, the total cluster energy will have to jump from E(N) to E(N+1). This gives rise to a peak in $\Delta_2(N)$. A peak in $\Delta_2(N)$ then indicates that a cluster is relatively stable. The stability suggests that this cluster should have a larger abundance in the mass spectrum than a cluster with N+1 or N-1 atoms.

In Fig 8, the calculated $\Delta_2(N)$ for lithium, sodium, and potassium is shown for N up to 95. The peaks in $\Delta_2(N)$ appear at N = 8, 18, 20, 34, 40, 58 and 92, with the filled orbitals indicated in the Figure. This is consistent with the experimental mass spectra discussed above.

To close this Section we show in Figure 9 ionization potentials of Li, Na and K clusters calculated in the spherical jellium model. These

predictions reproduce the drops associated with the closing of electronic shells (see figure 2). However, the jellium predictions overestimate the oscillations of IP with size.

4. SHELL EFFECTS IN LARGE CLUSTERS

Shown in Fig. 10 are the charge density, effective potential and energy-level structure for some Sodium clusters with filled shells, obtained by Ekardt[10]. The gaps between energy levels become smaller as the number of electrons increases. Eventually these energy levels will evolve into the energy bands of the solid when N is sufficiently large. When this occurs? or, in other words, when shell effects are not discernible any more? Some estimations[11] indicate shell effects to remain important up to a size of a few thousand atoms. Recent experiments shed some light into this problem.

The mass spectra of very large clusters yield anomalies which still can be explained as a consequence of the filling of high electronic shells. Figure 11 shows the abundance distribution obtained by Bjønrholm[12] for large Sodium clusters in an adiabatic expansion using Krypton as carrier gas. The spectra has a bell-shaped envelope modulated by a sawtooth like fine structure. The envelope reflects the global kinetics of cluster growth during the high-pressure phases of the expansion, while the fine structure is interpreted as being due to shell structure. The sawtooth steps become gradually more rounded as one proceeds towards higher masses. First of all, with an increasing number of shells, confined to an energy interval about equal to the Fermi energy (3.24 eV for Na), the gaps at the closed shells will diminish. Secondly at finite temperatures electrons can be excited across the gaps, and this tends to smear out the shell structure. The local features of the abundance spectra can be displayed more clearly by taking the logarithmic derivative of the intensity values, d ln I_N/dN. This is shown in the bottom panel. The magic numbers determined experimentally in this way are indicated in the figure. To the series already known one must add N = 138, 196, 260±4, 344±4, 440±2 and 558±8. The uncertainties are due to the reasons discussed above.

Results for even larger sodium clusters have been obtained by Martin and coworkers[13].Two mass spectra are shown in Fig. 12. Notice the strong dependence of these spectra on the wavelength of the ionizing light. The first three step-like features in the top spectrum correspond to sodium clusters containing 340, 440, and 560 atoms. By successively increasing the wavelength of the ionizing light, the cluster signal for low masses disappears and the step-like features at high masses sharpen. Although the first two steps in the mass spectrum taken with 400 nm laser light are quite well defined, features at higher masses are characterized by rather broad minima. There features have been identified in the figure. Martin's experiments reveal the sharp decrease of the ionization potential (increase in the number of counts) which occurs between Na_N and Na_{N+1} when Na_N is a closed-shells cluster. In the range below N = 600 Martin obtained agreement with Bjørnholm. Furthermore, additional anomalies were observed at N = 700±15, 840±15, 1040±20, 1220±20 and 1430±20 (see Table 1 for the complete list).

An interesting observation in figure 12 is that the magic numbers appear at approximately equal intervals when the mass spectra are plotted on a $N^{1/3}$ rather than N scale ($N^{1/3}$ gives the linear dimensions of the clusters). This behaviour can be explained by the following argument. When the number of electrons in the cluster increases, also the number of electronic shells increases, (see Figure 10). Theoretical

calculations have shown that the energy levels group together in bunches with empty gaps in between[13,14]. One can already see this effect in the simple examples of Figure 4. The 2d, 1h and 3s levels of the square well potential bunch closely together and substantial gaps "only" occur between this group and the 1g shell, o between this group and the nex bunch of levels, formed by 2f, 1i and 3p. But, do theoretical calculations for large clusters produce the precise bunching of energy levels required to explain the magic numbers observed by Bjørnholm[12] and Martin[13]?

Handling such a large number of electrons makes the calculation rather difficult. Two theoretical calculations have been performed which (a) lead to the bunching effect, that is, the $N^{1/3}$ periodicity, and (b) give magic numbers in rather good agreement with experiment.

These two calculations are now briefly dicussed. The results of the first calculation, performed by Nishioka et al[14], are shown in Fig. 13. This figure gives the energy for electrons moving in a spherical Woods-Saxon potential with parameters appropriate to sodium clusters. Of course, the volume of the binding field is proportional to the number of constituents N in the clusters. Adding the single particle energy eigenvalues of this potential leads to a sum E(N):

$$E(N) = \sum_{j=1}^{N} \varepsilon_j = E_{av}(N) + E_{shell}(N), \qquad (13)$$

where the main trend is a smooth part, $E_{av}(N)$, which is the sum of a negative volume term, proportional to N, and a (positive) surface term, proportional to $N^{2/3}$. Superimposed to this is an oscillating term, $E_{shell}(N)$. This $E_{shell}(N)$ is the energy actually plotted in Figure 13. The downward cusps represent shell closings, occurring at magic numbers.

The results of the second calculation, performed by Martin et

al[13,15] are included in Table 1 under the heading "jellium", and also in Figure 14. However, to obtain the required sequence of magic numbers (reflected here in the drops of the ionization potential) the jellium background had to be deformed a little, by making the clusters more dense in its inner part. This is also indicated in Fig.14, and the justification for this model will be provided later on in these lectures.

We can understand qualitatively why shell structure should occur at approximately equal intervals on an $N^{1/3}$ scale. Notice that an expansion of N in terms of the shell index K will always have a leading term proportional to K^3. One power of K arises because we must sum over all shells up to K in order to obtain the total number of particles. One power of K arises because the number of subshells in a shell increases approximately linearly with shell index. Finally, the third power of K arises because the number of particles in the largest subshell also increases with the shell index. then

$$N_K \approx K^3 \qquad (14)$$

where N_K is the total number of particles needed to fill all shells up to and including K.

The bunching of subshells is also observed in other problems. For instance, in the hydrogen atom subshells for which $k+l$ have the same value are degenerate. Subshells of the spherical harmonic oscillator for which $2k+l$ have the same value are also degenerate. For this reason it is said that these systems have quantum numbers $k+l$ and $2k+l$ that determine the energy. The results in Table 1 indicate that $3k+l$ is an approximate quantum number for alkali metal clusters. The total number of particles needed to fill all shells k up to and including $K = 3k + l$ is not difficult to evaluate, although the result is rather

awkard to write as a general formula. The leading term is

$$N_K = \frac{2}{9} K^3 + \ldots \qquad (15)$$

that is, cubic in K as expected. Table 1 shows that the shells in sodium clusters do not obey exactly the rule K = 3k+l but that this is however, a good approximation. These qualitative arguments give support to the more quantitative results of Figures 13 and 14.

5. THE SPHEROIDAL MODEL

Apparently the detailed configuration of the atomic arrangement in simple metal clusters does not seem to play an important role in the study of their physical properties We have seen that the spherical assumption is very successful in correlationg the prominent features of the mass spectra. However, there is evidence of many small features which the spherical assumption is unable to explain. Whenever a top-shell is not completely filled (N≠ 2, 8, 20, 40, 58, 92), the electronic density becomes non-spherical, which in turn leads to an ellipsoidal distortion of the ionic background. This Jahn-Teller type distortion, similar to those obseved for molecules and nuclei, leads to a splitting of all electronic spherical shells into spheroidal sub-shells[16]. Ellipsoidal clusters are prevalent for open-shell configurations.

Assuming major axes a and b for an ellipse, a distortion parameter η can be defined

$$\eta = \frac{2(a - b)}{a + b} \qquad (16)$$

Clemenger[17] has studied the effect of the ellipsoidal deformations for alkali clusters with N less than 100, using a modified three dimensional harmonic oscillator model. The model considers different oscillation frequencies along the z axis (taken as axis of symmetry)

and perpendicular to the z axis. The model Hamiltonian used by Clemenger also contains an anharmonic term. Its purpose is to flatten the botton of the potential well and to make it to resemble a rounded square-well potential similar to those shown in Figs 4 (center) or 10.

The deformation parameter η describes how prolate or oblate the cluster is. This distortion parameter is determined by minimizing the total energy calculated by summing the electronic eigenvalues of occupied states. For alkali clusters with N less than 100, values up to η = 0.5 are estimated for open shell clusters. This model appears to be adequate to explain many of the features of these systems. The main first-order effects of the ellipsoidal model are energy shifts that are proportional to η. These lead to fine structure in the mass spectrum. The stability function $\Delta_2(N)$ obtained in this model has, in addition to the peaks that appear in Fig. 8, many smaller subshell-filling peaks. These give rise to fine structure features at N = 10, 14, 18, 26, 30, 34, 36, 38, 44, 46, 50, 54, etc. The results are plotted in Figure 15, where they are compared with experimental abundances. Thermodynamic arguments establish the relation[1]:

$$\ln \frac{I_N^2}{I_{N+1} I_{N-1}} = \frac{\Delta_2(N)}{KT} \qquad (17)$$

where I_N are the detected intensities and T is the nozzle temperature. Consequently, instead of plotting just the intensities I_N (as in fig.1) we have plotted the left hand side of eq. (17). All the fine-structure peaks predicted by $\Delta_2(N)$ are observed experimentally (except N = 18), and some additional ones (12, 17, 23, 43). Some examples of the agreement in Fig. 15 follow: The fourfold patterns in the 1f and 1g shells appear correctly, and the fwofold patterns in the 2p shell correspond to the filling of a prolate subshell at 36 and an oblate

shell at 38.

The spherical jellium model described in Section 3 has been recently extended by Ekardt and Penzar[16,18] to account for spheriodal deformations. In this model the ionic background is represented by a distribution of positive charge with constant density and a distorted, spheroidal, shape. The advantage with respect to Clemenger's model[17] is that the spheroidal jellium model is parameter-free and that the calculation of the electronic wave functions is performed self-consistently. Results for Δ_2, ionization potentials and dissociation energies of Na clusters as a function of N reproduce well the experimental trends. As an example Fig. 16 shows the unimolecular decay of $Na_N^+ \rightarrow Na_{N-1}^+ + Na$.

6. FORMATION OF VERY LARGE CLUSTERS. TRANSITON TO THE BULK?

The recent experiments porformed by Martin, Bergman, Göhlich and Lange[13], just described in Section 4 above, give additional interesting information.

We have seen that when the mass spectra of large Na_N clusters are plotted versus $N^{1/3}$, the magic numbers appear at approximately equal intervals. However, Fig. 12 already shows that the period of appearance of these features changes abruptly in the size region 1400-2000 atoms. A new periodicity then appears which can be observed in the size region $1500 < N < 22.000$ (see Figures 12 and 17). According to Martin this new sequence reflects the filling of shells of atoms. For small clusters there is no problem in imagining that the cluster shape changes each time an electron is added, that is, the shape accomodates to the electron configuration and viceversa. This

is the essential message from the spheroidal model. However, as the size increases, changes in global cluster shape become more and more difficult. A new growth pattern must emerge. The clusters most probably grow by adding shells of atoms to a rigid core.

The number of atoms contained in a growth shell is dependent on the preferred coordination and local symmetry of the atoms and on the overall symmetry of the shell. If we assume that the sodium atoms are close-packed, or nearly so, and that the outer form is that of a cuboctahedron or an icosahedron, then the total number of atoms N_K in a cluster containing K shells of atoms is[20]

$$N_K = \frac{2}{3} (10 K^3 - 15 K^2 + 11 K - 3) \qquad (18)$$

These numbers are in very good agreement with the set of minima observed in the mass spectra of large sodium clusters (Fig. 17).

On the other hand it is believed that structures in the mass spectra obtained by Martin reflect size dependent variations in the ionization energy of the clusters. The reason for this is that these structures are dependent on the wavelength of the ionizing laser light. How can the atomic shell structure be related with the ionization energies? A very simple argument is the following. Clusters with closed atomic shells have high symmetry and therefore highly degenerate electronic states at the Fermi energy. If the symmetry is lowered by adding a partial shell of atoms, the degeneracy is lifted, splitting the states at the Fermi energy into higher and lower energy states. Therefore, clusters with closed shells of atoms have higher ionization energies than clusters with partial shells of atoms.

Why might one expect a transition from electronic shell structure to shells of atoms? For very small clusters the atoms are highly mobile. There is no difficulty for the atoms to arrange themselves

into a sphere-like conformation if this is demanded by the closing of an electronic shell. That is, small clusters behave like droplets. Each time an atom is added, it is absorbed into the droplet. At a size corresponding to about 1500 atoms under the experimental conditions of Martin's experiments, the cluster solidifies. Thereafter, each newly added atom condenses onto the surface and remains there. Further growth takes place by the accumulation of shells of atoms. The magic numbers observed in Martin's experiments indicate that these shells could be either cuboctahedra or icosahedra. Notice finally that bulk sodium is body centred cubic but an hexagonal-close- packed phase has been prepared at very low temperature [21].

REFERENCES

1.- W.A. de Heer, W. D. Knight, M.Y. Chou and M.L. Cohen, Solid State Phys. 40, 93 (1987).

2.- W. D. Knight, K. Clemenger, W.A. de Heer, W.A. Saunders, M.Y. Chou and M. L. Cohen, Phys. Rev. Lett. 52, 2141 (1984)

3.- M.M. Kappes, Chem. Rev. 88, 369 (1988)

4.- N.D. Bhaskar, R.P. Frueholz, C.M. Klimcak and R.A Cook, Chem. Phys. Lett. 154, 175 (1989)

5.- N.D. Bhaskar, C.K. Klimcak and R.A. Cook, Phys. Rev. B 42, 9147 (1990)

6.- C. Bréchignac, Ph. Cahuzac, F. Carlier, M. de Frutos and J. Leygnier, J. Chem. Soc. Faraday Trans. 86, 2525 (1990)

7.- R.D. Woods and D.S. Saxon, Phys. Rev. 95, 577 (1954)

8.- Electrons in Metals and Alloys. J.A. Alonso and N.H. March, Academic Press, London (1989)

9.- Theory of the Inhomogeneous Electron Gas, Eds. S. Lundqvist and N.H. March, Plenum Press, New York (1983)

10. W. Ekardt, Phys. Rev. B 29, 1558 (1984)

11.- S. Bjørnholm, Contemp. Phys. 31, 309 (1990)

12.- S. Bjørnholm, J. Borggreen, O. Echt, K. Hansen, J. Pedersen, and H.D. Rasmussen, Phys. Rev. Lett. 65, 1629 (1990)

13.- T.P. Martin, T. Bergmann, H. Göhlich and T. Lange, Z. Phys. D (April 1991)

14.- H. Nishioka, K. Hansen and B. Mottelson, Phys. Rev. B 42, 9377 (1990)

15.- T. Lange, H. Göhlich, T. Bergmann and T.P. Martin, Z. Phys. D (April 1991)

16.- W. Ekardt and Z. Penzar, Phys. Rev. B 38, 4273 (1988)

17.- K. Clemenger, Phys. Rev. B 32, 1359 (1985)

18.- Z. Penzar and W. Ekardt, Z. Phys. D 17, 69 (1990)

19.- C. Bréchignac, Ph. Cahuzac, J. Leygnier and J. Weiner, J. Chem Phys. 90, 1492 (1989)

20. A.L. Mackay, Acta Crystall. 15, 916 (1962)

21. C.S. Barret, Acta Crystall. 9, 67 (1956)

CAPTIONS OF FIGURES

Figure 1. Mass spectrum of sodium clusters showing shell structure.

Figure 2. Experimental K cluster ionization potentials. The bulk work function is 2.4 eV.

Figure 3. Dissociation energies of the lowest dissociation channel of K_N^+ and Na_N^+ (obtained from photodissociation experiments).

Figure4. Energy level spectra for three spherically symmetric potential wells: a three dimensional isotropic harmonic oscillator (left), a square-well potential (right) and a potential intermediate between these two (center). The energy labels (with degeneracies in parentheses) and the total number of states are given.

Figure 5. Due to the Pauli principle and to electrostatic repulsion, one electron creates a hole around it, that is, a region where other electrons have difficulties to penetrate. Here we show the pair distribution function in a homogeneous electron gas characterised by $r_s = 2$. r_s is related to the density n of the homogeneous electron gas by $(4/3)\ \pi\ r_s^3 = n^{-1}$

Figure 6. Self-consistent electron potential, calculated for a spherical cluster with twenty atoms. The single electron levels are also shown. Filled circles indicate electrons occupying the lowest levels. The open circle shows where the 21st electron would have to go. The jellium model was used in this calculation.

Figure 7. Calculated total energy per atom in the spherical jellium model for sodium as a function of cluster size.

Figure 8. Relative stability function, $\Delta_2(N)$, versus N for lithium, sodium and potassium. The labels correspond to filled shell orbitals.

Figure 9. Ionization potentials of Li, Na and K clusters calculated using the spherical jellium model. The values for a semi-infinite jellium (planar surface) are 3.37, 3.06 and 2.74 eV for Li, Na and K respectively.

Figure 10. Electron charge density, effective potential, and eigenvalues for two closed-shells sodium clusters. Calculations were performed by Ekardt[10] within the jellium model.

Figure 11. Top panels: abundance distributions for sodium clusters produced by adiabatic expansion and measured by time -of- flight mass spectrometry. Botton panels: logarithmic derivative of results in top panels.

Figure 12. Mass spectra of Na_N clusters photoionized with 400 and 410 nm light. The y axis denotes the total number of counts accumulated in a 40 μsec time channel after about 10^5 laser shots. Two sequences of structures are observed at equally spaced intervals on the $N^{1/3}$ scale.

Figure 13. The periodically varying contribution from valence electrons to the binding energy of a spherical sodium cluster. Magic numbers are indicated.

Figure 14. Ionization potential calculations using an inhomogeneous jellium model.

Figure 15. (a) Measured neighboring cluster abundances, compared with (b) total energies from the spheroidal model[1].

Figure 16. Comparison between theory and experiment for the binding energy D (in eV) for the unimolecular decay of $Na_N^+ \rightarrow Na_{N-1}^+ + Na$. All major shell closings are clearly seen. Experimental results are from Bréchignac et al[19]. Theoretical results are obtained by the spheroidal jellium model of Ekardt and Penzar[18].

Figure 17. Averaged mass spectra of Na_N clusters photoionised with 415 and 423 nm light. Well defined minima occur at values of N corresponding to the total number of atoms in close packed cuboctahedra and nearly-close-packed icosahedra (listed at top)[13].

TABLE I: TOTAL NUMBER OF ELECTRONS IN CLOSED SHELL CLUSTERS

Shell	Experiment	Jellium	Pseudo q.n.
A	2	2	2
B	8	8	8
C	18	18	18
D	20	(20)	
E	34	34	34
F	40	(40)	
G	58	58	58
H	90		90
I	92	92	
J	138	134	132
K	198 ± 2	(196)	186
L	263 ± 5	(268)	252
M	341 ± 5	338	332
N	443 ± 5	440	428
O	557 ± 5	562	540
P	700 ± 15	704	670
Q	840 ± 15	852	820
R	1040 ± 20		990
S	1220 ± 20		1182
T	1430 ± 20		1398

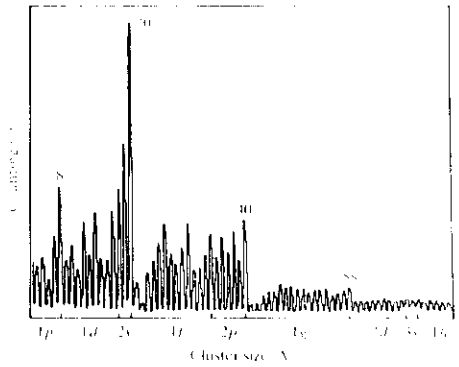

Figure 1. Mass spectrum of sodium clusters showing shell structure From Knight *et al.* (1984).

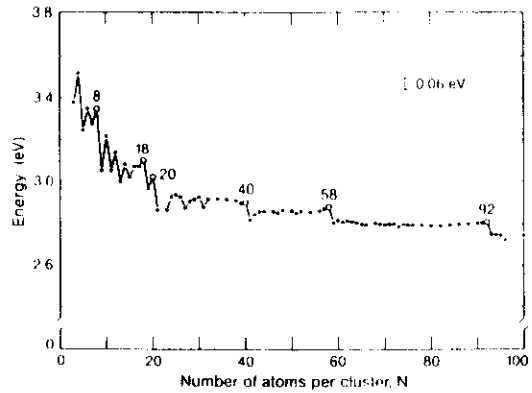

FIG. 2. Experimental K cluster ionization potentials. The bulk work function is 2.4 eV

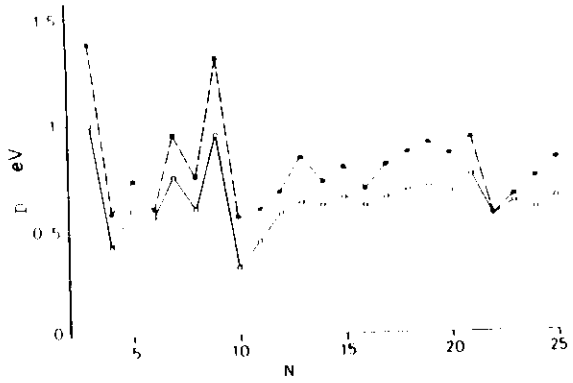

Fig. 3. Dissociation energies of the lowest dissociation channel for Na^{+}_{N} (●) and K^{+}_{N} (○) *versus* N

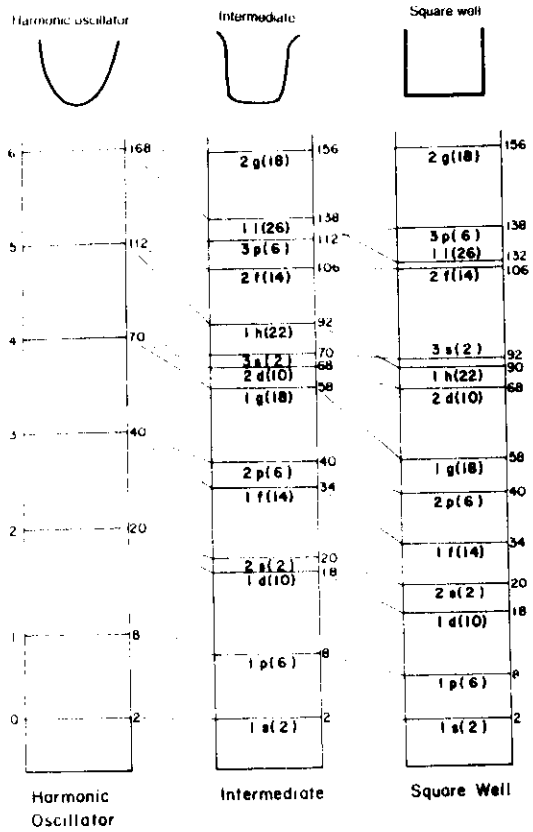

Fig. 4. Order of energy levels of the electrons trapped in a harmonic oscillator, a square well and an intermediate potential between them. The energy is not to scale. The figures in parentheses represent the number of degenerate levels and the figures at the right hand side of the levels represent the total number of levels counted from the lowest level (shell-closing number).

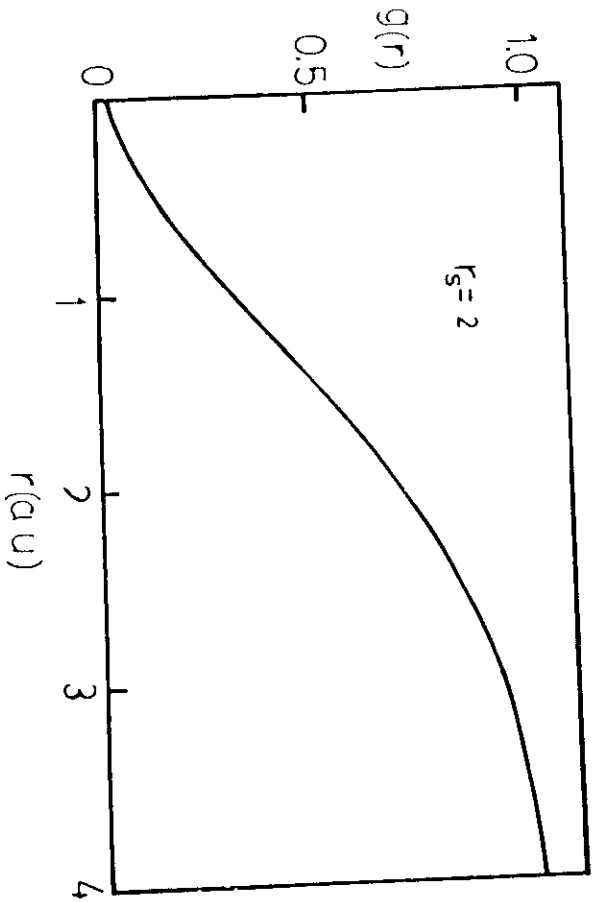

Fig. 5

Figure 6. self-consistent electron potential, calculated for a spherical sodium cluster with twenty atoms. The calculated single-electron energy levels are also shown. Filled circles indicate electrons occupying the lowest levels; the open circle shows where a 21st electron would have to go. In this calculation, the positive sodium ions are assumed to form a uniform, positive, spherical charge distribution with a sharp surface and a density equal to the bulk density of sodium metal (Jellium model).

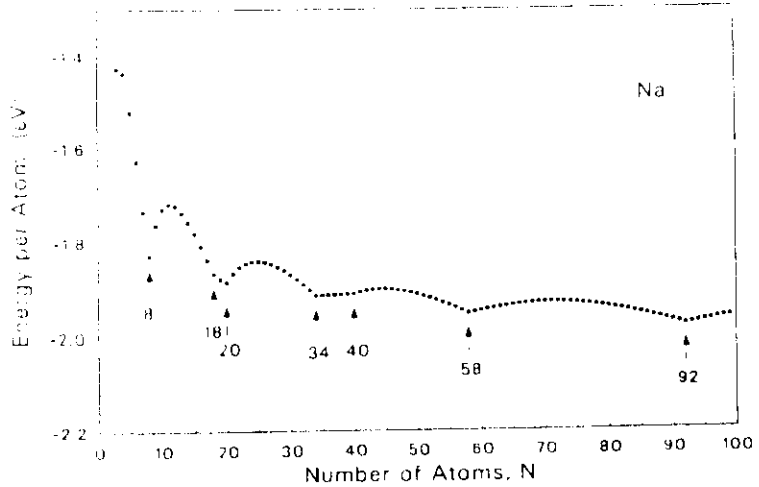

Fig. 7 The calculated total energy per atom in the spherical jellium model for sodium (r_s = 3.93 a.u.) as a function of cluster size.

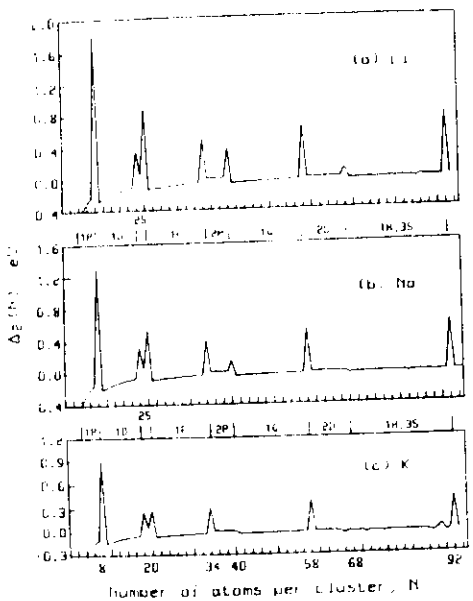

FIG. 8 The relative binding energy change $\Delta_2(N)$ versus N, the number of atoms per cluster for (a) lithium, (b) sodium, and (c) potassium. The labels correspond to filled shell orbitals.

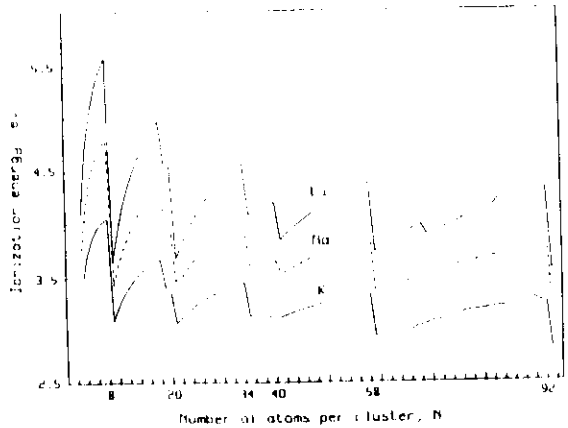

FIG. 9 Theoretical ionization potential for Li, Na, and K. The calculated work functions of the infinite half plane jellium surface for Li, Na, and K are 3.37, 3.06, and 2.74 eV, respectively.

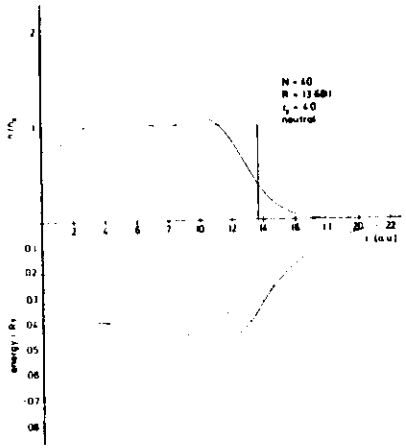

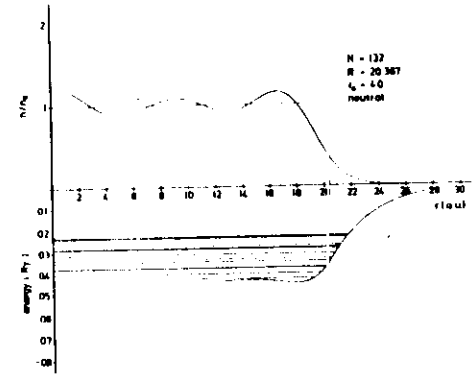

Fig. 10

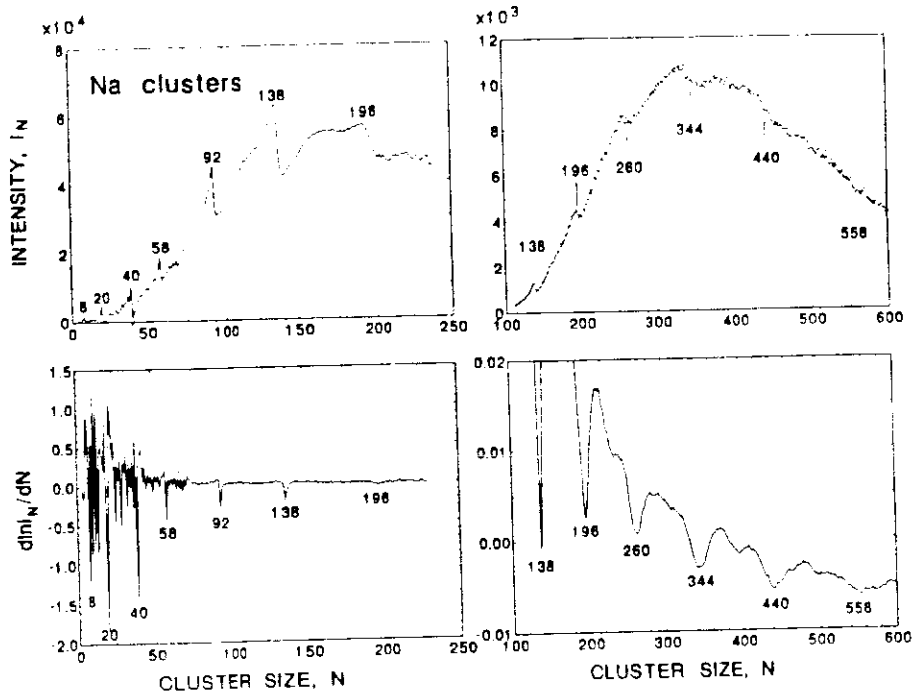

FIG 11 Top panels: Abundance distributions for sodium clusters produced by adiabatic expansion and measured by time-of-flight mass spectrometry. Bottom panels: Logarithmic derivative of results in top panels

Fig. 12

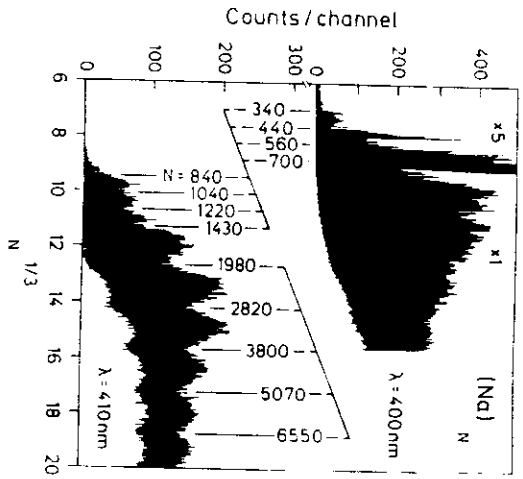

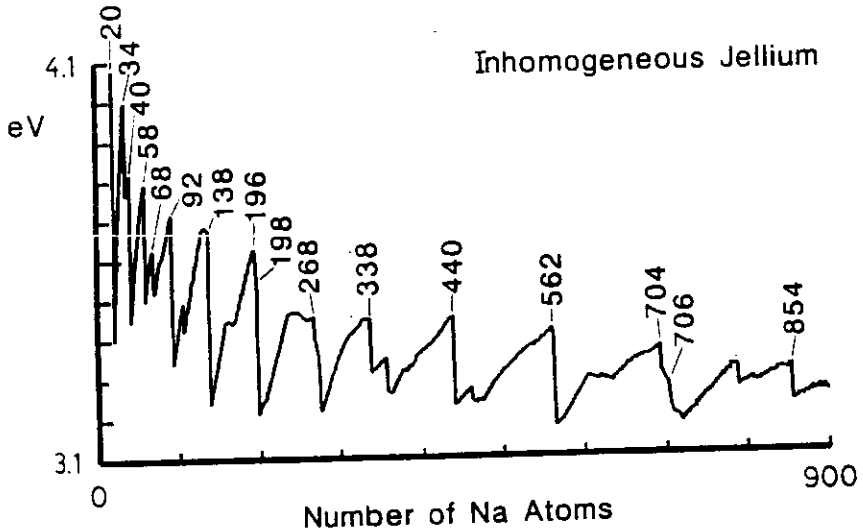

F-g. 14

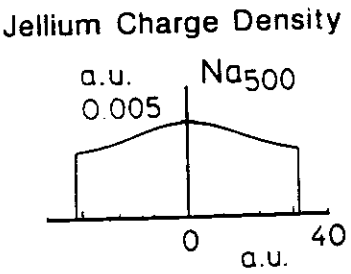

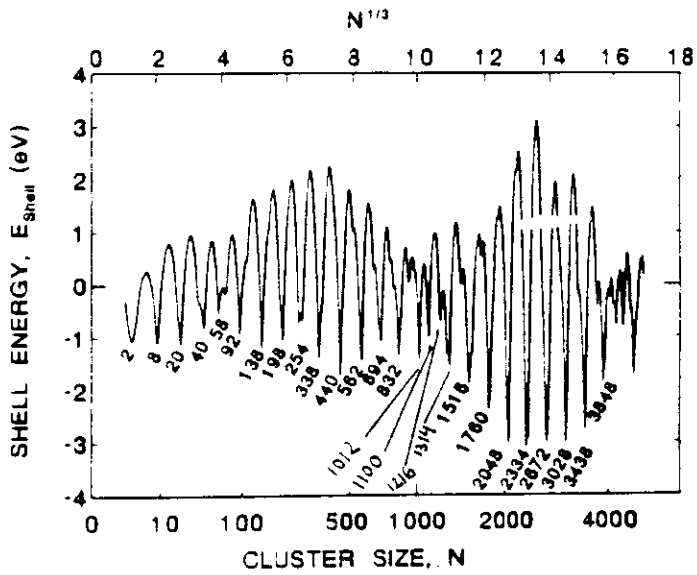

FIG. 13. The periodically varying contribution from valence electrons to the binding energy of a spherical sodium cluster. Magic numbers are indicated.

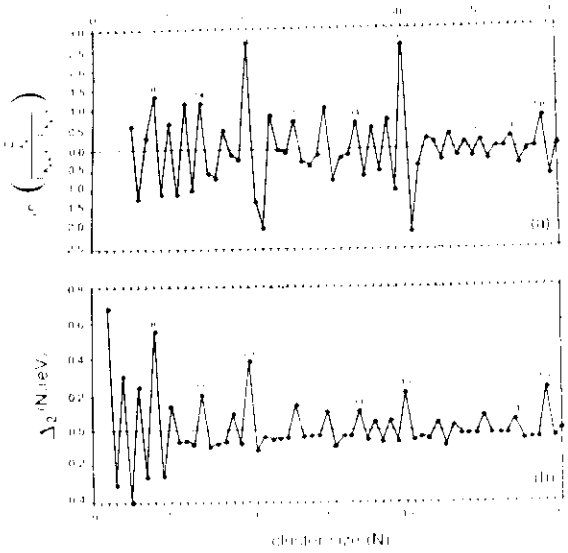

FIG. 15 (a) Measured neighboring cluster abundances, compared with (b) total energies

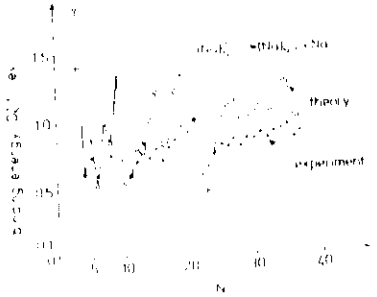

Fig. 16 Comparison between theory and experiment by C. Bréchignac et al. for the binding energy D_n of the neutral Na_n for the unimolecular decay of $(Na_n)^+ \rightarrow (Na_{n-1})^+ + Na$

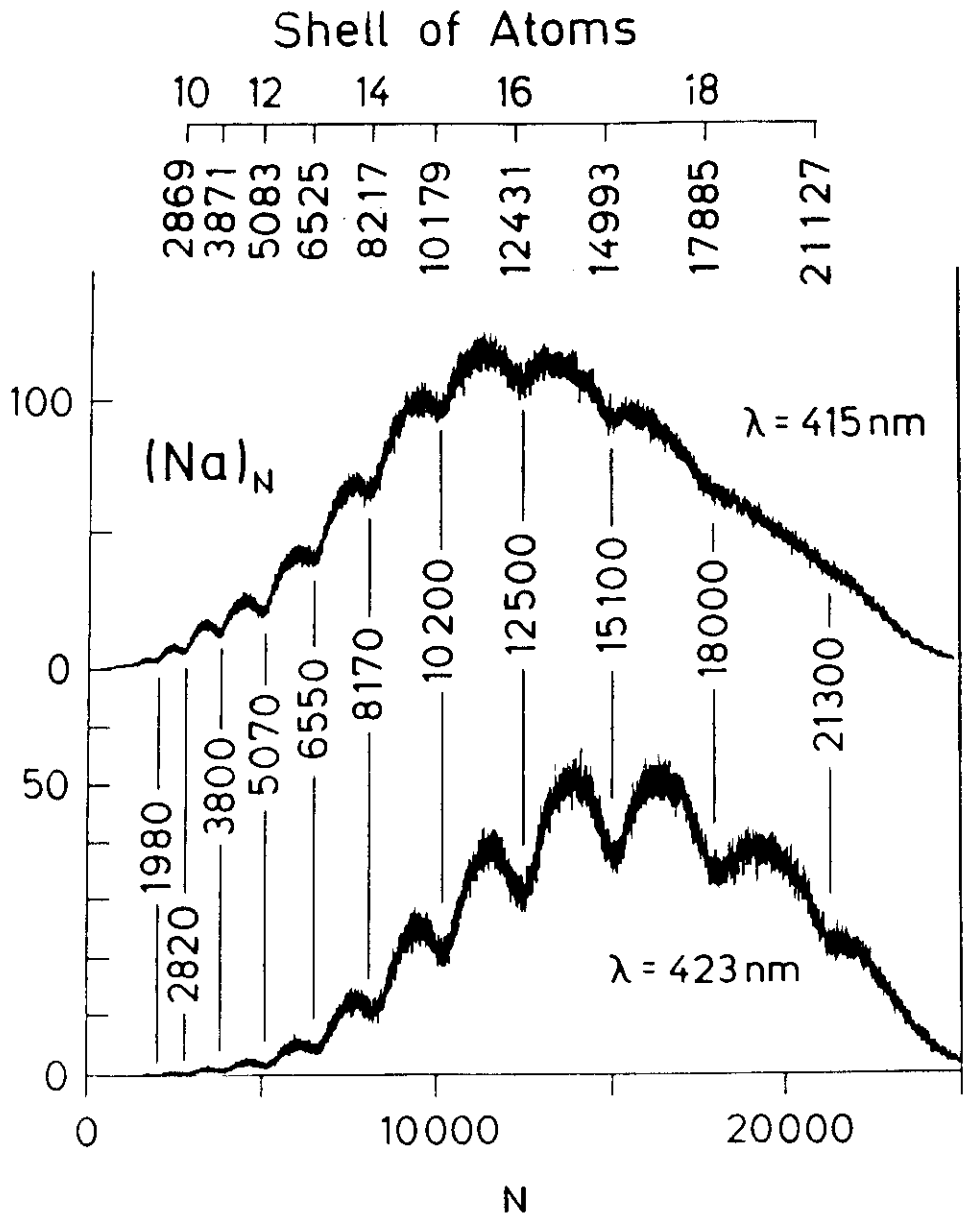

Fig. 17